Cancer Cell
Article

A BCL6/BCOR/SIRT1 Complex Triggers Neurogenesis and Suppresses Medulloblastoma by Repressing Sonic Hedgehog Signaling

Luca Tiberi,[1] Jérôme Bonnefont,[1] Jelle van den Ameele,[1] Serge-Daniel Le Bon,[1] Adèle Herpoel,[1] Angéline Bilheu,[1] Beverly W. Baron,[2] and Pierre Vanderhaeghen[1,3,*]
[1]Université Libre de Bruxelles (ULB), Institute for Interdisciplinary Research (IRIBHM), and ULB Institute of Neuroscience (UNI), 808 Route de Lennik, 1070 Brussels, Belgium
[2]Department of Pathology, University of Chicago, Chicago, IL 60637, USA
[3]Walloon Excellence in Life Sciences and Biotechnology (WELBIO), Université Libre de Bruxelles, 808 Route de Lennik, 1070 Brussels, Belgium
*Correspondence: pierre.vanderhaeghen@ulb.ac.be
http://dx.doi.org/10.1016/j.ccell.2014.10.021

SUMMARY

Disrupted differentiation during development can lead to oncogenesis, but the underlying mechanisms remain poorly understood. Here we identify BCL6, a transcriptional repressor and lymphoma oncoprotein, as a pivotal factor required for neurogenesis and tumor suppression of medulloblastoma (MB). BCL6 is necessary for and capable of preventing the development of GNP-derived MB in mice, and can block the growth of human MB cells in vitro. BCL6 neurogenic and oncosuppressor effects rely on direct transcriptional repression of Gli1 and Gli2 effectors of the SHH pathway, through recruitment of BCOR corepressor and SIRT1 deacetylase. Our findings identify the BCL6/BCOR/SIRT1 complex as a potent repressor of the SHH pathway in normal and oncogenic neural development, with direct diagnostic and/or therapeutic relevance for SHH MB.

INTRODUCTION

During embryonic development, the balance between proliferation and differentiation, and the subsequent emergence of cellular diversity, depend on a delicate interplay between intrinsic and extrinsic cues. The same morphogenic pathways are often deregulated during oncogenesis (Taipale and Beachy, 2001), and indeed many tumors are thought to result from aberrant differentiation events, although in most cases the underlying mechanisms remain poorly understood. One striking example of the tight link between morphogenesis and oncogenesis is medulloblastoma (MB), the most prevalent malignant brain tumor in children. MB are thought to be caused at least in part by deregulation of pathways normally acting during brain development, such as WNT and Sonic Hedgehog (SHH) pathways (Parsons et al., 2011; Roussel and Hatten, 2011). Importantly the pathway at stake has a direct impact on the clinical features of the tumor, leading to the classification of MB into four major subgroups, with pathological features associated with specific molecular pathways (Kool et al., 2014; Northcott et al., 2012a, 2012b; Olson, 2014; Thompson et al., 2006). The SHH subtype accounts for approximately 25% of MB. SHH MB are caused mainly by aberrant gain of function of the SHH pathway (Northcott et al., 2012a). Indeed human SHH MB tumors are frequently associated with disruptive mutations of genes encoding negative regulators of SHH signaling, such as *PTCH1* or *SUFU*, or amplification of genes encoding SHH effectors or SHH target genes, such as *GLI2* or *MYCN* (Gilbertson and Ellison, 2008; Northcott et al., 2012a). MB are typically located in the cerebellum, in which granule neuron precursors (GNP) were found to constitute the main cells of origin of SHH MB in the mouse (Schüller et al., 2008; Yang et al., 2008).

Significance

There is tremendous interest today in the links between developmental pathways and oncogenesis. This is particularly relevant for tumors that are thought to be of developmental origin. Here we found that BCL6, a well-known lymphoma oncoprotein, acts as a key neurogenesis factor during normal cerebellar development and as a potent tumor suppressor for medulloblastoma. Remarkably, both effects rely on the same molecular mechanism of epigenetic repression of Sonic Hedgehog signaling effectors Gli1 and Gli2 through the recruitment of BCOR corepressor and SIRT1 deacetylase. Our data identify the BCL6/BCOR/SIRT1 complex as an important target of direct diagnostic and/or therapeutic relevance for SHH medulloblastoma.

The SHH pathway plays a crucial role in the normal development of the cerebellum, in particular in GNP (Fuccillo et al., 2006). In mice, SHH is normally secreted by Purkinje neurons in the developing cerebellum, where it promotes the expansion and maintenance of GNP through activation of Gli1 and Gli2 transcription factors, the main positive effectors of the SHH pathway (Corrales et al., 2006; Fuccillo et al., 2006). Interestingly, other factors involved in GNP development have been linked to MB oncogenesis, most strikingly the MATH1/Atoh1 transcription factor that is required for the specification and proliferation of GNP (Ben-Arie et al., 1997), while its disruption in the mouse results in a block of SHH MB development, mostly through transcriptional control of *Gli* genes (Dahmane and Ruiz i Altaba, 1999; Flora et al., 2009). Collectively these data provide a direct link between genes that promote specification and expansion of GNP and SHH MB oncogenesis. Conversely, the proneurogenic factors that promote the neurogenic conversion of GNP into granule neurons during normal in vivo development could provide leads toward MB oncosuppression, but their nature and mechanisms of action remain essentially unknown. BMP cues have been reported to be able to increase GNP neurogenesis in vitro, while inhibiting the oncogenic growth of human MB cells, but their requirement in any of these processes has not been tested (Grimmer and Weiss, 2008; Zhao et al., 2008). Similarly, proneural genes such as *Neurod1* and *Mash1* have been implicated in granule neuron differentiation (Alvarez-Rodríguez and Pons, 2009; Cho and Tsai, 2006), but their potential involvement in MB remains unexplored.

BCL6 is a transcriptional repressor involved in B cell development and oncogenesis (Basso and Dalla-Favera, 2012; Chang et al., 1996; Duy et al., 2011; Hurtz et al., 2011; Ye et al., 1993, 1997), but recently has been identified also as a proneurogenic factor in the developing cerebral cortex (Tiberi et al., 2012). Here, we explore the role of BCL6 during cerebellar neurogenesis and its involvement in MB oncogenesis.

RESULTS

BCL6 Is Expressed in GNP during Cerebellar Neurogenesis

To test the effect of BCL6 in neural cell populations, we surveyed its expression in the developing brain and found high levels of expression in the postnatal cerebellum. BCL6 was strongly expressed in the external granular layer (EGL), which contains GNP as well as differentiating granule neurons, and in the internal granular layer, containing postmigratory granule neurons (Figure 1A). Costainings for BCL6 and Ki67 (marker of proliferating GNP) or NeuN (marker of postmitotic granule neurons) revealed a partially overlapping pattern, with BCL6 expressed among Ki67$^+$ GNP (Figure 1B and Figure S1A available online) and early-born neurons in the EGL, as well as in differentiated NeuN$^+$ granule neurons in the internal granule layer (IGL) (Figures 1B and 1C). Calbindin$^+$ Purkinje cells did not express BCL6 (Figure S1B). Importantly, the specificity of BCL6 immunostaining was confirmed in each case using *Bcl6* knockout (KO) mice, which revealed no immunostaining (Figures 1D and S1C). These data indicate that BCL6 is expressed in GNP during their transition to a neuronal fate, consistent with a role during neurogenesis as in the cerebral cortex (Tiberi et al., 2012).

BCL6 Is Required for Proper GNP Neuronal Differentiation

We then examined *Bcl6* KO mice (Ye et al., 1997) and found decreased cerebellar size and weight at P21 (Figure S1D), suggesting a disruption of GNP proliferation, survival, and/or differentiation. The proliferation patterns of GNP were analyzed using pH3 and Ki67 stainings and did not reveal significant alteration in *Bcl6* KO mice at the time of neurogenesis (Figures S1A, S1C, S1E, and S1F). We then examined the number of NeuN$^+$ cells specifically in the EGL at P7, and we found a decrease in the newly born neurons in KO compared to wild-type (WT) (Figures 1C–1E) as well as a decrease in NeuN$^+$ IGL area (Figure 1F). Overall, these data strongly suggest a defect in the generation of granule neurons in the *Bcl6* KO mice.

We next performed EdU pulse-chase experiments combined with Ki67 staining and found a marked reduction of cell-cycle exit at P7 in the cerebellum of *Bcl6* KO mice, further confirming defective neurogenesis from GNP to postmitotic neurons (Figures 1G and 1H). Apoptosis, as determined by the number of cleaved caspase 3$^+$ cells, was increased in *Bcl6* KO mice at P7 (Figures S1G and S1H), suggesting aberrant neuronal specification. We then determined whether BCL6 was able to trigger GNP neurogenesis using a gain-of-function approach on ex vivo cultures of GNP. BCL6 overexpression resulted in a potent neurogenic effect, characterized by an increase in the number of NeuN$^+$ neurons generated after 72 hr (Figure S1I). Fluorescence-activated cell sorting (FACS) analysis using the anti-cleaved caspase 3 antibody revealed no difference in the percentage of apoptotic cells within the different conditions (percentage cleaved caspase 3$^+$ cells: Ctr, 3.30 ± 0.43; BCL6, 3.16 ± 0.68; n = 8; Figures S1J and S1K). Altogether these data indicate that BCL6 is required in vivo for the proper differentiation of GNP and it is able to trigger GNP neurogenesis in vitro.

BCL6 Acts as a Direct Repressor of SHH Effectors *Gli1* and *Gli2*

To gain insight into the underlying mechanisms, we examined gene expression among FACS-purified GNP populations in control and *Bcl6* KO mice at P7, using *Math1-GFP* knockin mice that express GFP exclusively in Math1$^+$ GNP (Figures 2A, 2B, and S2A; Rose et al., 2009). We focused our analysis on genes known to be involved in GNP proliferation and differentiation (Ben-Arie et al., 1997; Flora et al., 2009) as well as on known BCL6-target genes in other contexts, in particular *TP53* and *ATR* that are implicated in the physiological and oncogenic effects of BCL6 in B cell lineages (Phan and Dalla-Favera, 2004; Ranuncolo et al., 2007; Sakano et al., 2010; Tiberi et al., 2012). This revealed little difference in the levels of expression of most genes examined (including genes related to the BMP, WNT, and NOTCH pathways, as well as *Trp53* and *Atr*) in *Bcl6* KO compared to WT GNP, except a strong upregulation of *Gli1* and *Gli2,* the main effectors of the SHH pathway (Figures 2C and S2B). In addition, *Ccnd2*, which is a downstream target of BCL6 in B cells, was found to be upregulated in the *Bcl6* KO cells (Nahar et al., 2011), while *Cdkn1b*, which encodes the cyclin-dependent kinase inhibitor p27, was found to be downregulated in the *Bcl6* KO cells, reflecting defective cell cycle exit. Overall, these data indicate that the SHH pathway appears to be a major target of

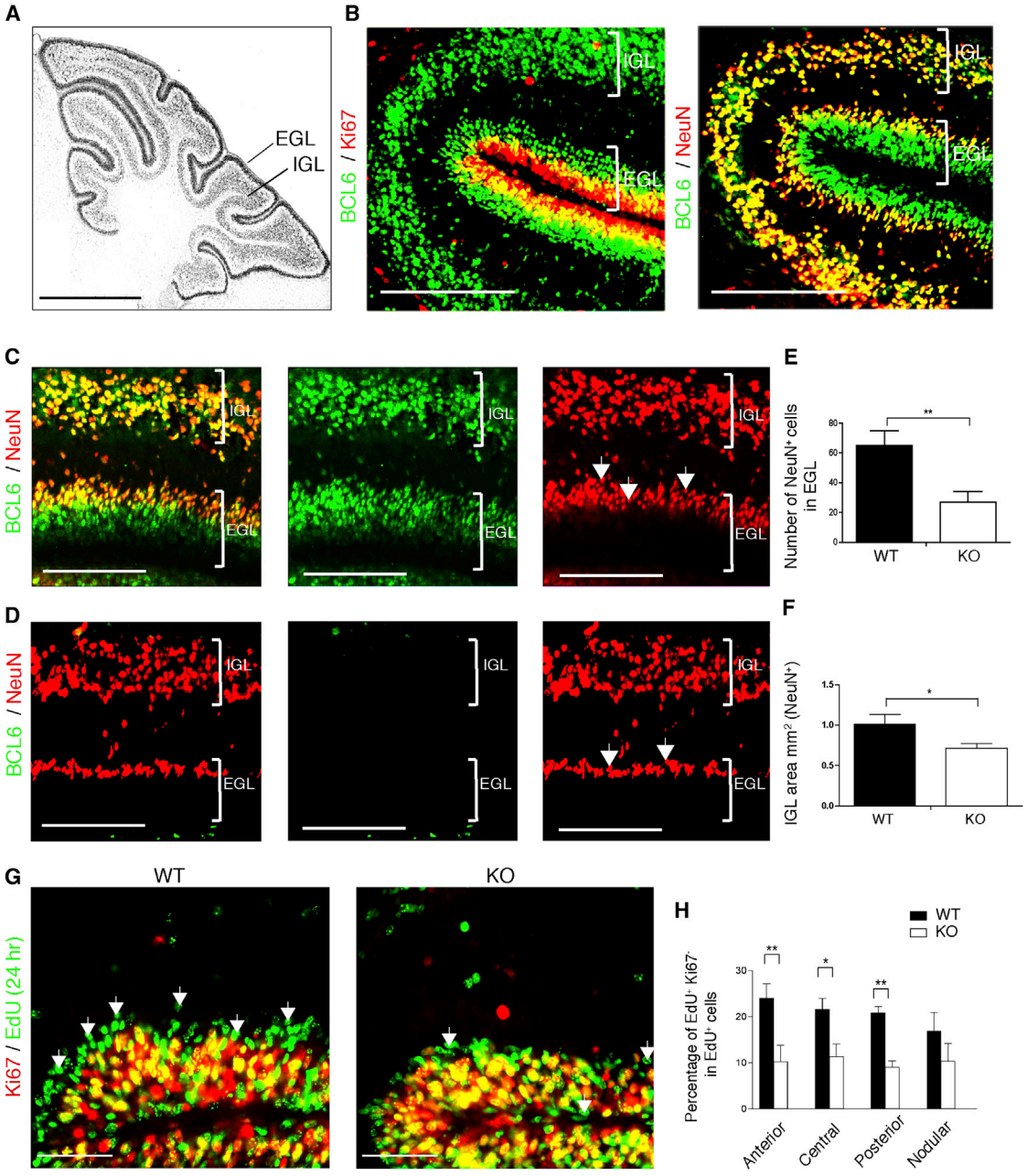

Figure 1. BCL6 Is Required for Proper Cerebellum Development

(A) Immunohistochemistry staining of sagittal sections of *Bcl6* WT cerebellum at P7 with BCL6 antibody. Scale bar, 1 mm.

(B) Confocal immunofluorescence staining for BCL6 with either Ki67 or NeuN of sagittal sections of P7 WT cerebellum. Scale bars, 250 μm.

(C and D) Confocal immunofluorescence staining for BCL6 and/or NeuN of sagittal sections of P7 WT (C) and *Bcl6* KO (D) cerebellum. Scale bars, 100 μm. Arrows point to $NeuN^+$ neurons in EGL.

(E) Quantification of the number of $NeuN^+$ cells in EGL *Bcl6* WT and KO brains at P7; n = 4.

(F) Quantification of the IGL area ($NeuN^+$ cells) of the cerebellum in *Bcl6* WT and KO brains at P7; n = 4, brains.

(G) Immunofluorescence analysis of sagittal sections of *Bcl6* WT and KO brains at P7 for EdU and Ki67. EdU was injected 24 hr before perfusion. Scale bars, 50 μm.

(H) Quantification of cell cycle exit index (EdU^+Ki67^-/EdU^+) in *Bcl6* WT and KO brains 24 hr after injection of EdU in four different regions of the cerebellum; n = 3.

Data are means ± SEM. Arrows point to EdU^+ $Ki67^-$ cells.

*p < 0.05, **p < 0.01. See also Figure S1.

BCL6 in the GNP lineage. Confirming this, BCL6 overexpression in GNP resulted in a strong repression of *Gli1* and *Gli2*, while most other tested genes remained unchanged (Figures 2D–2F).

We next examined whether *Gli1* and *Gli2* repression was causally linked to the proneurogenic effects of BCL6. The double knockdown of Gli1 and Gli2 resulted in increased

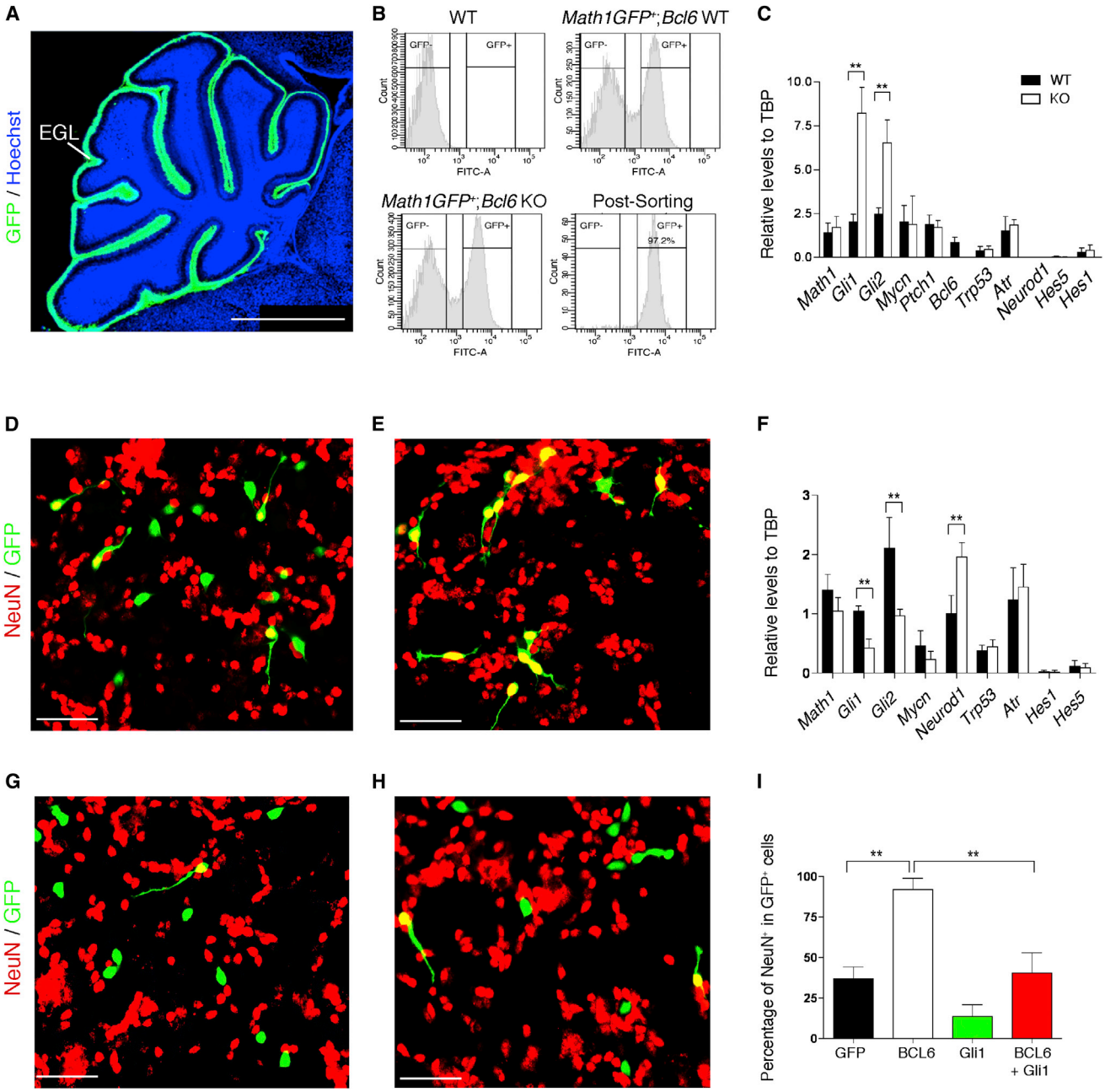

Figure 2. BCL6 Induces Neurogenesis through *Gli1* Repression

(A) Immunofluorescence staining for GFP and Hoechst of sagittal section of cerebellum from a *Math1-GFP*$^+$ mouse at P7. Scale bar, 1 mm.

(B) Representative FACS histograms showing GFP expression in cerebellar cells isolated from WT, *Bcl6* WT;*Math1-GFP*$^+$, and *Bcl6* KO;*Math1-GFP*$^+$ mice at P7. Postsort analysis was performed by reanalyzing the GFP profile of 10,000 sorted cells.

(C) Quantitative real-time PCR analysis for *Math1*, *Gli1*, *Gli2*, *Mycn*, *Ptch1*, *Bcl6*, *Trp53*, *Atr*, *Neurod1*, *Hes5*, and *Hes1* from FACS-sorted *Math1-GFP*$^+$ cells from *Bcl6* WT and KO cerebellum at P7; n = 3.

(D and E) Immunofluorescence analysis for GFP and NeuN, 72 hr after nucleofection with pCIG (D) or pCIG-BCL6 (E) of ex vivo culture of cerebellar cells from WT P7 mice. Scale bars, 50 μm.

(F) Quantitative real-time PCR analysis for *Math1*, *Gli1*, *Gli2*, *Mycn*, *Neurod1*, *Trp53*, *Atr*, *Hes5*, and *Hes1* from FACS-sorted GFP$^+$ cells 72 hr after nucleofection with pCIG or pCIG-BCL6 of ex vivo culture of cerebellar cells from WT P7 mice; n = 3.

(G and H) Immunofluorescence analysis for Hoechst, GFP, and NeuN, 72 hr after nucleofection with pCIG-Gli1 (G) or pCIG-BCL6 + pCIG-Gli1 (H) of ex vivo culture of cerebellar cells from WT P7 mice. Scale bars, 50 μm.

(I) Histograms show the percentage of cells expressing NeuN among all GFP+ cells 72 hr after nucleofection with pCIG, pCIG-BCL6, pCIG-Gli1, and pCIG-BCL6 + pCIG-Gli1 of ex vivo culture of cerebellar cells from WT P7 mice; n = 4.

Data are means ± SEM. *p < 0.05, **p < 0.01. See also Figure S2.

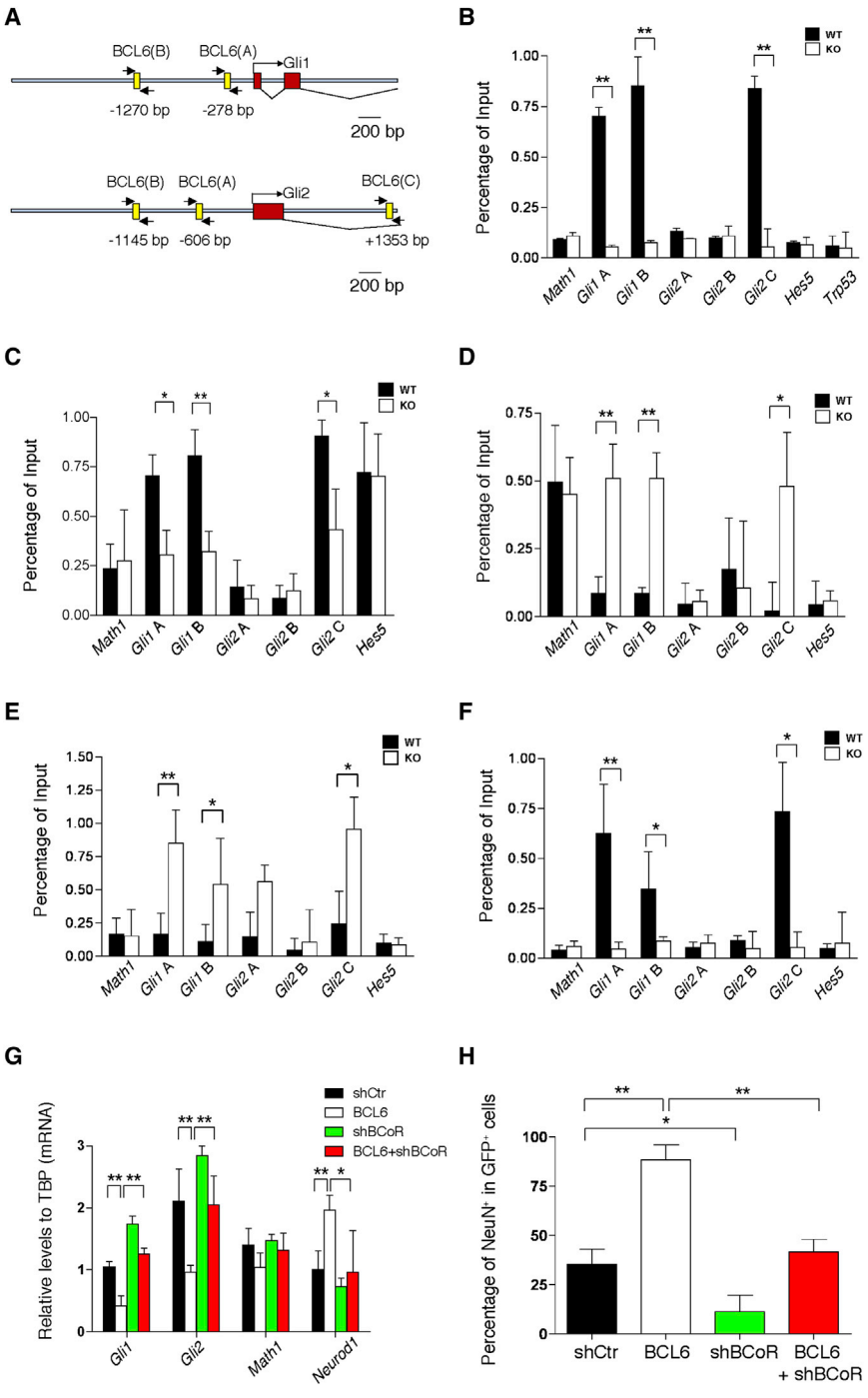

Figure 3. BCL6 Directly Represses *Gli1*/*Gli2* Expression

(A) Schematic representation of the genomic region of mouse *Gli1* and *Gli2*, showing the exons in red and the potential BCL6 binding sites in yellow. Primers used in ChIP assay are presented by thick arrows.

(B–F) ChIP analysis of the putative BCL6-binding sites in the *Math1*, *Gli1*, *Gli2*, *Hes5*, and *Trp53* promoters in *Bcl6* WT and KO cerebellar tissue at P7 with anti-BCL6 (B), SIRT1 (C), H1.4K26ac (D), H4K16ac (E), and BCOR (F) antibodies; n = 3.

(G) Quantitative real-time PCR analysis for *Gli1*, *Gli2*, *Math1*, and *Neurod1* from FACS-sorted GFP$^+$ cells 72 hr after nucleofection with pCIG + pSCV2-shCtr, pCIG-BCL6 + pSCV2-shCtr, pCIG + pSCV2-shBCoR, and pCIG-BCL6 + pSCV2-shBCoR of ex vivo culture of cerebellar cells from WT P7 mice; n = 3.

(H) Histograms show the percentage of GFP$^+$ cells expressing NeuN 72 hr after the nucleofection with pCIG + pSCV2-shCtr, pCIG-BCL6 + pSCV2-shCtr, pCIG + pSCV2-shBCoR, and pCIG-BCL6 + pSCV2-shBCoR of ex vivo culture of cerebellar cells from WT P7 mice; n = 3.

Data are means ± SEM. *p < 0.05, **p < 0.01. See also Figure S3.

GNP neurogenesis, thus mimicking BCL6 gain of function (Figure S2C–S2E), while overexpression of Gli1 together with BCL6 completely blocked BCL6-dependent neurogenesis (Figures 2D–2I). These data indicate that BCL6 exerts its effects in GNP by repressing SHH effectors, raising the question of the underlying molecular mechanism. In silico inspection of *Gli1* and *Gli2* regulatory regions revealed the presence of several BCL6 binding sites located close to the transcriptional starting points (Figure 3A). Using BCL6-chromatin immunoprecipitation (ChIP) experiments from WT and *Bcl6* KO P7 cerebellum, we found a specific enrichment directly in two sites in the *Gli1* promoter and in one site in the *Gli2* first intron, while no enrichment could be detected in putative binding sites located in *Hes5*, *Math1*, or *Trp53* promoters (Figure 3B). These data indicate that BCL6 repression on *Gli1* and *Gli2* likely reflects a direct action on their regulatory regions.

BCL6 Neurogenic Activity Requires SIRT1 Deacetylase and BCOR Corepressor

We previously found that BCL6 can repress transcription by recruiting the SIRT1 deacetylase (Tiberi et al., 2012). Using coimmunoprecipitation (coIP) on P7 mouse cerebellar extracts, we detected BCL6 in the same complex as SIRT1 (Figure S3A). ChIP experiments on chromatin prepared from cerebellar tissue at P7 revealed that SIRT1 was enriched at the BCL6 binding site of the *Gli1* and *Gli2* promoters, and that this enrichment was markedly reduced in *Bcl6* KO cerebellum (Figure 3C), whereas the total levels of SIRT1 appeared to be unchanged (Figure S3A). We next determined whether BCL6/SIRT1 could influence chromatin acetylation patterns at the *Gli1* and *Gli2* regulatory regions. ChIP analysis revealed strong enrichment of acetylated H1.4K26Ac and H4K16Ac on *Gli1* and *Gli2* promoters in *Bcl6* KO P7 cerebellum compared with WT (Figures 3D and 3E). Thus, the chromatin around

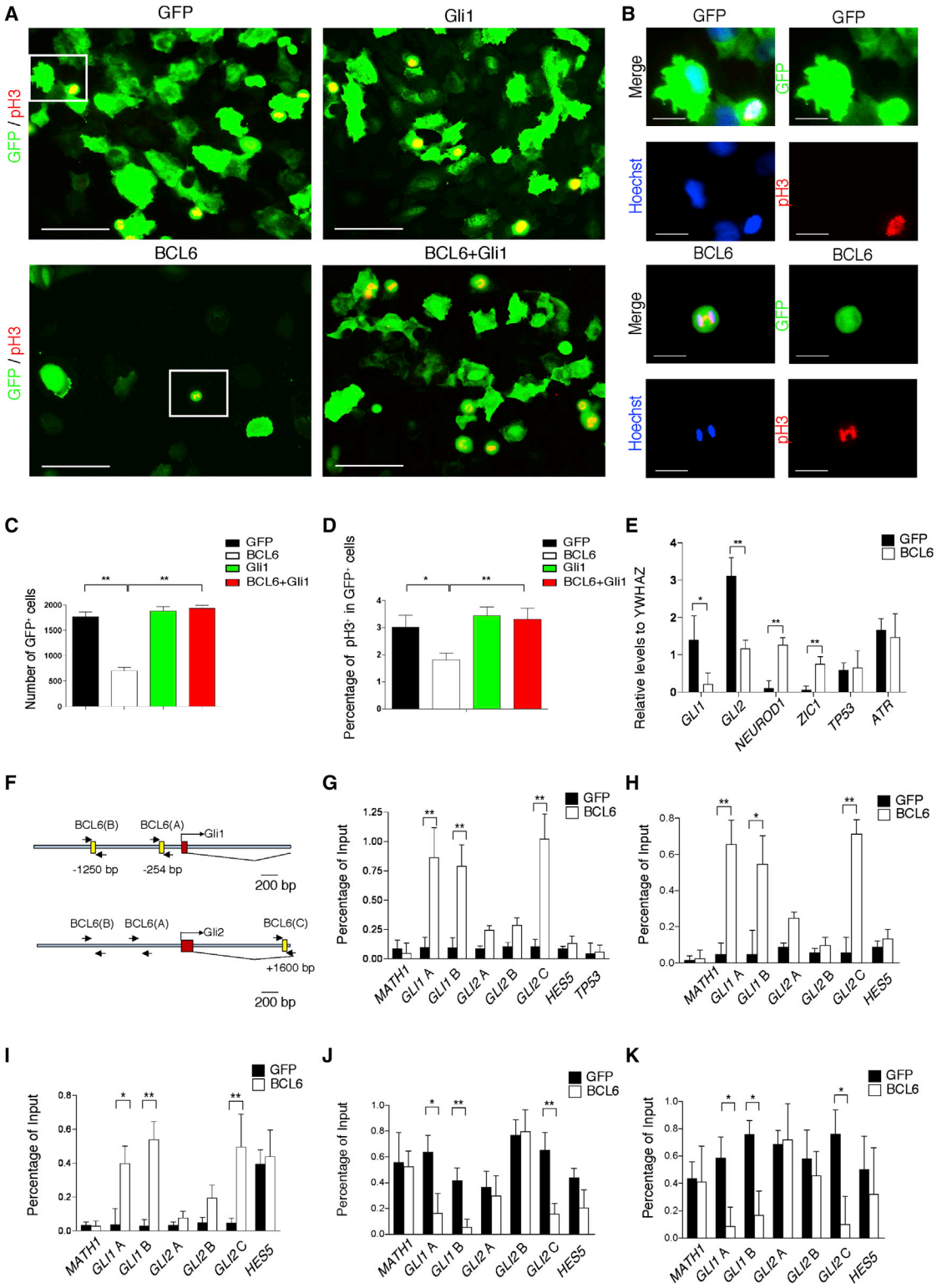

Figure 4. BCL6 Represses DAOY Cells Proliferation through *Gli1* Repression

(A) Immunofluorescence staining for GFP and pH3 of DAOY cells 5 days after nucleofection with pCIG, pCIG-Gli1, pCIG-BCL6, and pCIG-BCL6 + pCIG-Gli1. Scale bars, 60 μm.

(B) Higher magnification of immunofluorescence staining for GFP and/or pH 3, Hoechst of panel (A). Scale bars, 20 μm.

(C) Histograms show the number of GFP$^+$ cells 5 days after the nucleofection of DAOY cells with pCIG, pCIG-BCL6, pCIG-Gli1, and pCIG-BCL6 + pCIG-Gli1; n = 4.

(legend continued on next page)

the *Gli1* and *Gli2* promoters was remodeled in a BCL6-dependent manner.

BCL6 also previously was shown to repress transcription through direct interactions with NCOR corepressor complex proteins, in particular BCOR (Huynh and Bardwell, 1998; Huynh et al., 2000). To test BCOR's contribution, we first performed coIP and found that BCOR bound BCL6 in the cerebellum (Figure S3B). Using ChIP, we observed recruitment of BCOR to the *Gli1* and *Gli2* promoters in the cerebellum, which was strongly decreased in *Bcl6* KO mice compared to control (Figure 3F). Furthermore, coIP demonstrated the presence of BCOR in the same complex as SIRT1 and this interaction was strongly reduced in *Bcl6* KO mice (Figure S3C**)**. To test the relevance of these findings to neurogenesis, we next knocked down BCOR in GNP during BCL6-induced neurogenesis, which completely abolished the ability of BCL6 to repress *Gli1* and *Gli2* (Figures 3G and S3D) and to induce neurogenesis in cultured GNP (Figures 3H and S3E). We then treated GNP with the SIRT1 inhibitor EX-527 (Min et al., 2010), which also resulted in the complete block of neurogenesis induced by BCL6 (Figure S3F). These data indicate that BCL6 converts GNP into neurons through the recruitment of BCOR and SIRT1 at the *Gli1* and *Gli2* promoters. We also tested the effect of BCOR overexpression or SIRT1 activation alone on ex vivo cultures of GNP (Figures S3G and S3H). No effect could be detected on neurogenesis, suggesting that the upregulation of BCL6, but not of BCOR or SIRT1, is a key event during GNP neurogenesis.

BCL6/BCOR/SIRT1 Complex Suppresses Growth of Human MB Cells through *Gli1 and Gli2* Repression

As aberrant activation of SHH signaling in GNP is thought to be at the origin of SHH MB (Schüller et al., 2008; Yang et al., 2008), we next examined the potential implication of BCL6 in their growth and development. We first tested the effects of BCL6 on the human MB DAOY cell line (Wang et al., 2012), which is sensitive to SHH pathway inhibition (Figures S4A and S4B). Overexpression of BCL6 in DAOY cells resulted in strong suppression of their growth and mitotic activity (Figures 4A–4D), as well as increased expression of neural differentiation markers, while *TP53*/*ATR* remained unaffected (Figure 4E). Cell apoptosis did not appear to be affected (Figure S4C; percentage cleaved caspase 3^+ cells: Ctr, 2.23 ± 0.25; BCL6, 1.89 ± 0.18; n = 8). Importantly, the tumor cell growth inhibitory effect was associated with *GLI1* and *GLI2* repression (Figure 4E), and was completely abrogated by coexpression of Gli1 (Figures 4A–4E), thereby linking repression of *GLI* genes to the growth suppressive effects of BCL6.

In line with this, we tested whether the antigrowth effect of BCL6 was specific to SHH-sensitive MB cell lines. We examined the effects of BCL6 on the human MB cell line D341-MED, which was proposed to be derived from a group 3 MB (Snuderl et al., 2013), and could not detect any effect of BCL6 or cyclopamine, in conditions similar to those used for DAOY cells, on these cells (Figures S4D–S4F). In silico inspection of the human *GLI1* and *GLI2* regulatory regions revealed the presence of two bona fide BCL6 binding sites in *GLI1* promoter region (like in the mouse) and only one in the *GLI2* promoter region (instead of three as in the mouse)(Figure 4F). We next performed ChIP analyses for BCL6, BCOR, and SIRT1 in DAOY cells following expression of BCL6 (Figures 4G–4I**).** This revealed that overexpressed BCL6 was strongly enriched at both *GLI1* and *GLI2* promoters, like in the mouse, while no enrichment could be found in other target gene promoters, such as *HES5* and *TP53* (Figure 4G). Moreover, BCL6 overexpression triggered the recruitment of BCOR and SIRT1 to *GLI1* and *GLI2* promoter regions, which was associated with decreased histone acetylation patterns (Figures 4H–4K). Importantly, the effects of BCL6 on repressing *GLI1* expression and MB cell growth were completely blocked following either BCOR knockdown (Figures 5A–5D and S5A) or SIRT1 knockdown and inhibition (Figures S5B–S5H). Also, BCOR knockdown effects were fully rescued by overexpressing the WT BCOR but not a BCOR mutant devoid of its putative BCL6 binding site (Figures 5A–5E) that was recently identified in SHH MB (Jones et al., 2012). Altogether these data indicate that BCL6, acting together with SIRT1/BCOR complexes, can repress *GLI1* and *GLI2* expression and thereby suppress the growth of a human SHH MB cell line.

BCL6 Overexpression Inhibits the Development of SHH MB In Vivo

To validate these findings in vivo, we turned to a well-established mouse model of SHH MB (Schüller et al., 2008), where a constitutively active mutant form of SHH effector Smo (SmoM2) can be selectively expressed in the GNP lineage, by crossing *Rosa26SmoM2* mice (Jeong et al., 2004) with *Math1-creER* mice (Machold and Fishell, 2005). Using this model, SmoM2 induction at P4 resulted in GNP overgrowth and MB-like, highly proliferating tumors in all cases examined (Figures 6A–6C). We then tested the effect of BCL6 overexpression using a mouse model that allowed doxycyclin- (Dox-)inducible ubiquitous expression of human BCL6 by crossing *tet-o-BCL6* mice (Baron et al., 2004) with *Rosa26 rtTA* (Hochedlinger et al., 2005; Figure 6D). Strikingly, the mice that overexpressed SmoM2 together with BCL6 showed a strong reduction in tumor formation at P14 (Figure 6E), together with a decreased proliferation (Figure 6F) and an increased expression of neuronal differentiation markers (Figures 6B, 6C, and 6E). Furthermore, Kaplan-Meier analysis revealed a doubling of the survival time following overexpression of BCL6, despite ongoing SmoM2 expression ($p < 0.001$;

(D) Histograms show the percentage of GFP^+ cells expressing pH 3, 5 days after the nucleofection of DAOY cells with pCIG, pCIG-BCL6, pCIG-Gli1, and pCIG-BCL6 + pCIG-Gli1; n = 4.

(E) Histograms show quantitative real-time PCR analysis for *GLI1*, *GLI2*, *NEUROD1*, *ZIC1*, *TP53*, and *ATR* 5 days after nucleofection of DAOY cells with pCIG or pCIG-BCL6; n = 4.

(F) Schematic representation of the genomic region of human *GLI1* and *GLI2*, showing the exon in red and the BCL6 binding sites in yellow. Primers used in ChIP assay are presented by thick arrows.

(G–K) ChIP analysis of the putative BCL6-binding sites in the *MATH1*, *GLI1*, *GLI2*, *HES5*, and *TP53* promoters and introns in DAOY cells nucleofected with pCIG or pCIG-BCL6 with anti-BCL6 (G), BCOR (H), SIRT1 (I), H1.4K26ac (I), and H4K16ac (K) antibodies; n = 3.

Data are means ± SEM. *$p < 0.05$, **$p < 0.01$. See also Figure S4.

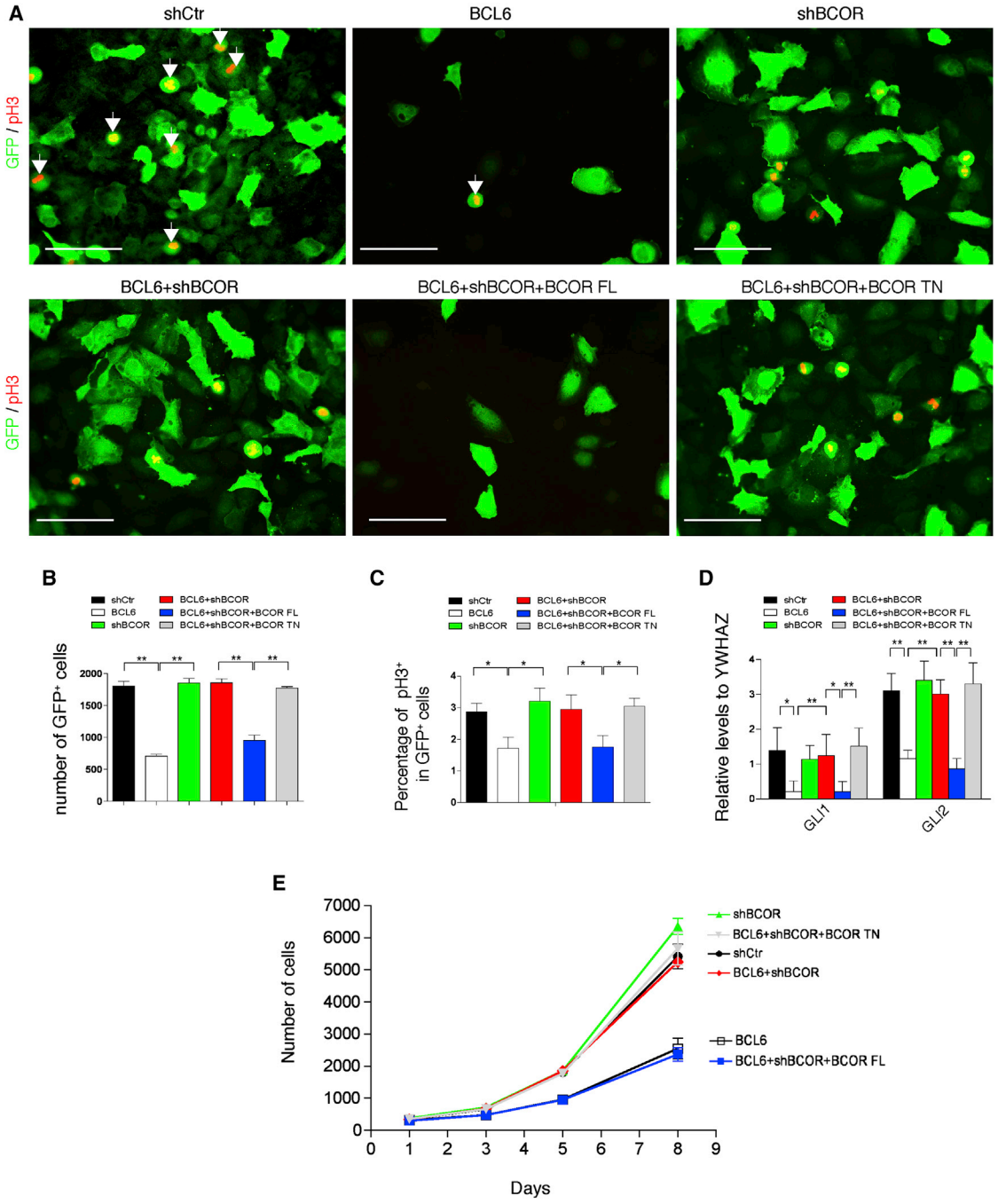

Figure 5. BCL6 Requires BCOR to Repress Proliferation of DAOY Cells

(A) Immunofluorescence staining for GFP and pH 3 of DAOY cells 5 days after nucleofection with pCIG + pSCV2-shCtr, pCIG-BCL6 + pSCV2-shCtr, pCIG + pSCV2-shBCOR, pCIG-BCL6 + pSCV2-shBCOR, pCIG-BCL6 + pSCV2-shBCOR + pCIG-BCOR-FL (full-length), and pCIG-BCL6 + pSCV2-shBCOR + pCIG-BCOR-TN (truncated). Scale bars, 60 μm. Arrows point to GFP^+ pH 3^+ cells.

(B–D) Histograms show the number of GFP^+ cells (B), the percentage of GFP^+ cells expressing pH 3 (C), or quantitative real-time PCR analysis for *GLI1* and *GLI2* (D) 5 days after nucleofection of DAOY cells with pCIG + pSCV2-shCtr, pCIG-BCL6 + pSCV2-shCtr, pCIG + pSCV2-shBCOR, pCIG-BCL6 + pSCV2-shBCOR, pCIG-BCL6 + pSCV2-shBCOR + pCIG-BCOR-FL (full-length), and pCIG-BCL6 + pSCV2-shBCOR + pCIG-BCOR-TN (truncated); n = 4.

(E) Graph shows quantification of GFP^+ cells after nucleofection of DAOY cells with pCIG + pSCV2-shCtr, pCIG-BCL6 + pSCV2-shCtr, pCIG + pSCV2-shBCOR, pCIG-BCL6 + pSCV2-shBCOR, pCIG-BCL6 + pSCV2-shBCOR + pCIG-BCOR-FL (full-length), and pCIG-BCL6 + pSCV2-shBCOR + pCIG-BCOR-TN (truncated); n = 4.

Data are means ± SEM. *$p < 0.05$, **$p < 0.01$. See also Figure S5.

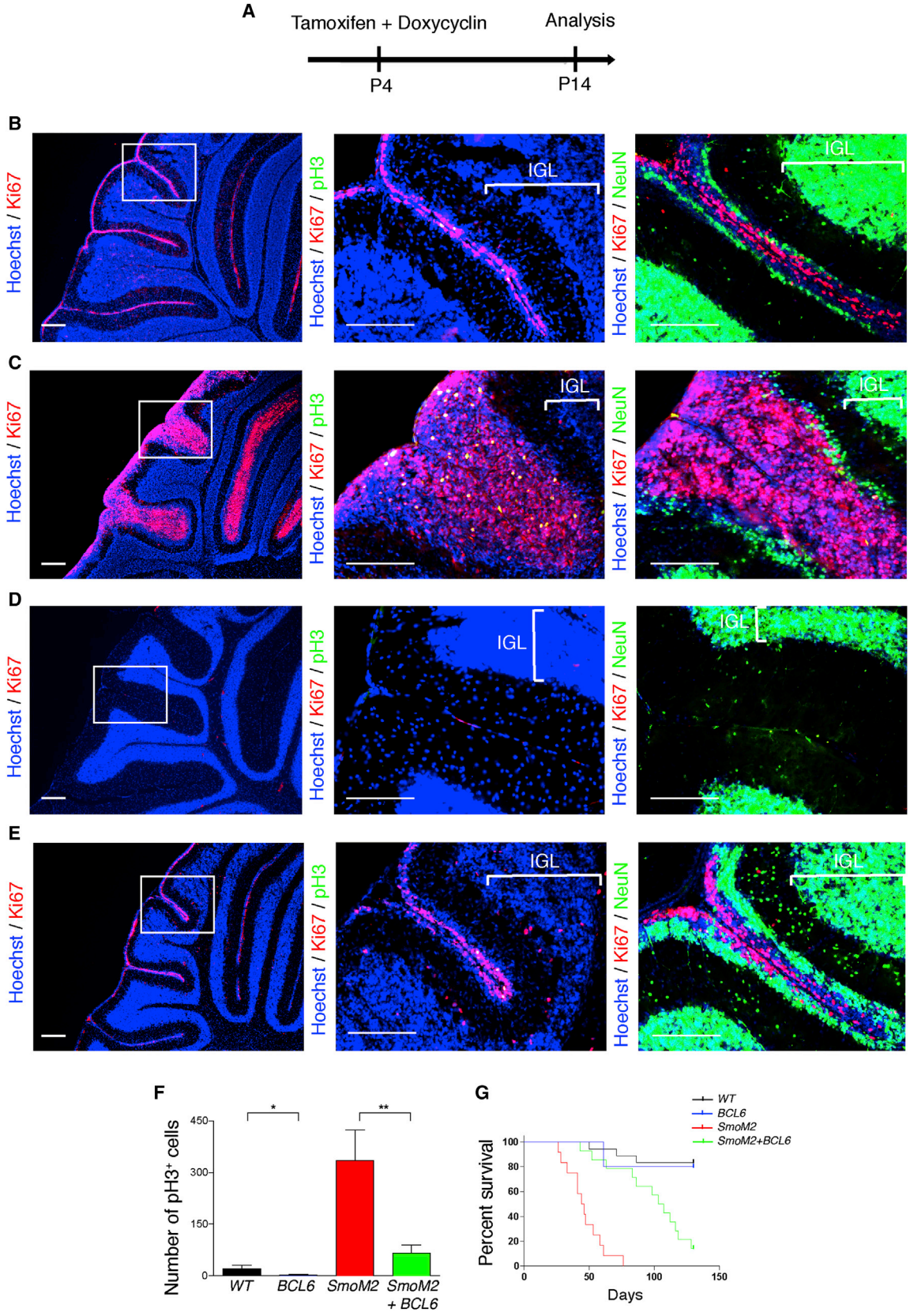

(legend on next page)

Figure 6G). Interestingly, BCL6 overexpression also resulted in suppression of proliferation in the EGL in mice without SmoM2 activation, suggesting that BCL6 acts similarly on normal and oncogenic proliferative patterns of GNP (Figure 6F). We then characterized in more detail the pattern of expression of BCL6 and Gli1 in this context (Figure S6A). BCL6 was found to be expressed 2 days following Dox injection (Figures S6B–S6E), including in the internal compartment of the tumor, while Gli1 was repressed following BCL6 induction (Figures S6F–S6I). In contrast, at P14 (thus 7 days following Dox induction), ectopic expression of BCL6 in the internal compartment of the tumor was no longer detectable (Figures S6J–S6M), while Gli1 was expressed in the tumor (Figures S6N–S6Q).

We next tested whether BCL6 also is able to reduce the growth of a tumor that is already established. For this purpose, we induced transient ectopic BCL6 expression 10 days after the SmoM2 activation (Figure 7A). This resulted in strong reduction in tumor growth (Figures 7B–7E), decreased proliferative patterns (although not to control levels) (Figure 7F), and increased survival time ($p < 0.001$; Figure 7G). This also increased expression of neuronal differentiation markers together with repression of *Gli1* and *Gli2*, while *Trp53* and *Atr* remained unchanged (Figures 7B–7E and 7H). We then characterized in more detail the pattern of expression of BCL6 and Gli1 in this context (Figure S7A). BCL6 was found to be expressed 2 days following Dox injection (Figures S7B–S7E), including in the internal compartment of the tumor, while Gli1 was repressed following BCL6 induction (Figures S7F–S7H). In contrast, by P21 (Figures S7I–S7N) and P40 (Figures S7O–S7T), 7 and 26 days following Dox induction, respectively, ectopic expression of BCL6 in the internal compartment of the tumor was no longer detectable (Figures S7B, S7I–S7K, and S7O–S7Q), while Gli1 was largely expressed throughout the tumor (Figures S7L–S7N and S7R–S7T). Finally, given the transient nature of BCL6 overexpression, we tried to test the effect of more sustained overexpression of BCL6 by performing experiments where Dox was injected several times (at P14, P16, P18, and P20), following tumor induction at P4. However, no ectopic expression of BCL6 could be detected beyond 2 days following induction, and, conversely, no additional increase in the survival of the mice could be obtained, when compared with the data obtained with a single injection at P14 (data not shown).

Overall, these data indicate that BCL6 transient overexpression can strongly delay and inhibit MB formation and development in vivo. BCL6 appears to act not only by reducing the pool of GNP but also by reducing the growth of established tumors, in part by promoting differentiation and possibly through other mechanisms, such as reduced proliferation. However these effects are only transient, most likely because of the transient expression of the BCL6 transgene, which could explain tumor growth after longer periods following the Dox treatment. It will be interesting to design for future studies a model where BCL6 is expressed in a constitutive fashion in the tumor, to test whether and how the tumors would then escape its oncosuppressive effects.

BCL6 Is Required in GNP to Suppress SHH MB In Vivo

To test the importance of endogenous BCL6 during MB formation, we used a mouse model where BCL6 was inactivated specifically in the GNP lineage by crossing *Bcl6* conditional KO (*Bcl6*$^{lox/lox}$) (Kaji et al., 2012) with *Math1-creER* mice (Machold and Fishell, 2005) and with tamoxifen injection at E15.5. *Bcl6* conditional KO mice examined at P21 displayed a smaller cerebellum compared to WT, like the germline *Bcl6* KO (Figures S8A–S8C), but did not display any sign of tumor formation up to 12 weeks of age. We then combined *Bcl6* inactivation with disruption of *Trp53* to reveal tumor formation in the cerebellum (Wetmore et al., 2001). Although *Trp53* disruption alone does not lead to MB in the mouse (Marino et al., 2000; Romer et al., 2004; Wetmore et al., 2001), the combined disruption of *Bcl6* and *Trp53* resulted in cerebellar tumor formation in more than half (n = 5/9) of the mice examined at 12 weeks of age (Figures 8A–8I). The location of the tumors was consistently found at the periphery of the cerebellum, and overproliferation patterns together with strong expression of Gli1 and Mycn further suggested that they correspond to SHH MB (Figures 8G–8I and S8D–S8F). Importantly, no tumor was detected in any WT (n = 7), *Bcl6* KO (n = 8), or *Trp53* KO (n = 11) mice (Figures S8G and S8H and Table S1). Tumor mass was much increased by 20 weeks in *Trp53;Bcl6* double KO mice (n = 2/2) (Figures 8J–8O), while no tumor was detected in any WT (n = 1), *Bcl6* KO (n = 2), or *Trp53* KO (n = 2) mice. These data indicate that endogenous BCL6 is required to prevent MB formation in vivo, strongly suggesting that it acts as a genuine oncosuppressor (Gilbertson and Ellison, 2008).

DISCUSSION

Our data show that the BCL6 protein acts as an intrinsic neuronal differentiating factor and tumor suppressor through direct repression of SHH signaling in the GNP lineage. In each case, BCL6 was found to act through the same molecular mechanism, i.e., through the recruitment of BCOR corepressor and SIRT1 histone deacetylase, thereby leading to epigenetic repression of Gli1 and Gli2 SHH effectors. These parallels strikingly illustrate how the same pathway can act as a differentiating factor and as a tumor suppressor, as previously shown for other genes and tumors (Asselin-Labat et al., 2007; Batlle et al., 2005; Bossuyt et al., 2009; Emmenegger et al., 2013; Kouros-Mehr et al., 2008; Zhao et al., 2008). BCL6 mechanisms of action also

Figure 6. BCL6 Represses SHH MB Development

(A) Schematic representation of the experimental protocol. Mice were injected with tamoxifen and doxycyclin at P4 and analyzed at P14.

(B–E) Immunofluorescence staining for Hoechst, Ki67, and pH 3 or Hoechst, Ki67, and NeuN of sagittal sections of P14 WT (B), *SmoM2* (C), *tet-o-BCL6*$^+$ (D), or *SmoM2*;*tet-o-BCL6*$^+$ (E) mice after injection of tamoxifen and doxycyclin at P4.

(F) Quantification of pH 3$^+$ cells within the EGL at P14 in WT, *SmoM2*, *SmoM2*;*tet-o-BCL6*$^+$, and *tet-o-BCL6*$^+$ mice injected with tamoxifen and doxycyclin at P4; n = 4.

(G) Survival curve of WT (n = 17), *tet-o-BCL6*$^+$ (n = 5), *SmoM2* (n = 12), and *SmoM2*;*tet-o-BCL6*$^+$ (n = 14) mice injected with tamoxifen and doxycyclin at P4. All the mice are *Math1-creER*$^+$;*rtTA*$^+$. Scale bars, 200 μm. Data are means ± SEM. *$p < 0.05$, **$p < 0.01$. See also Figure S6.

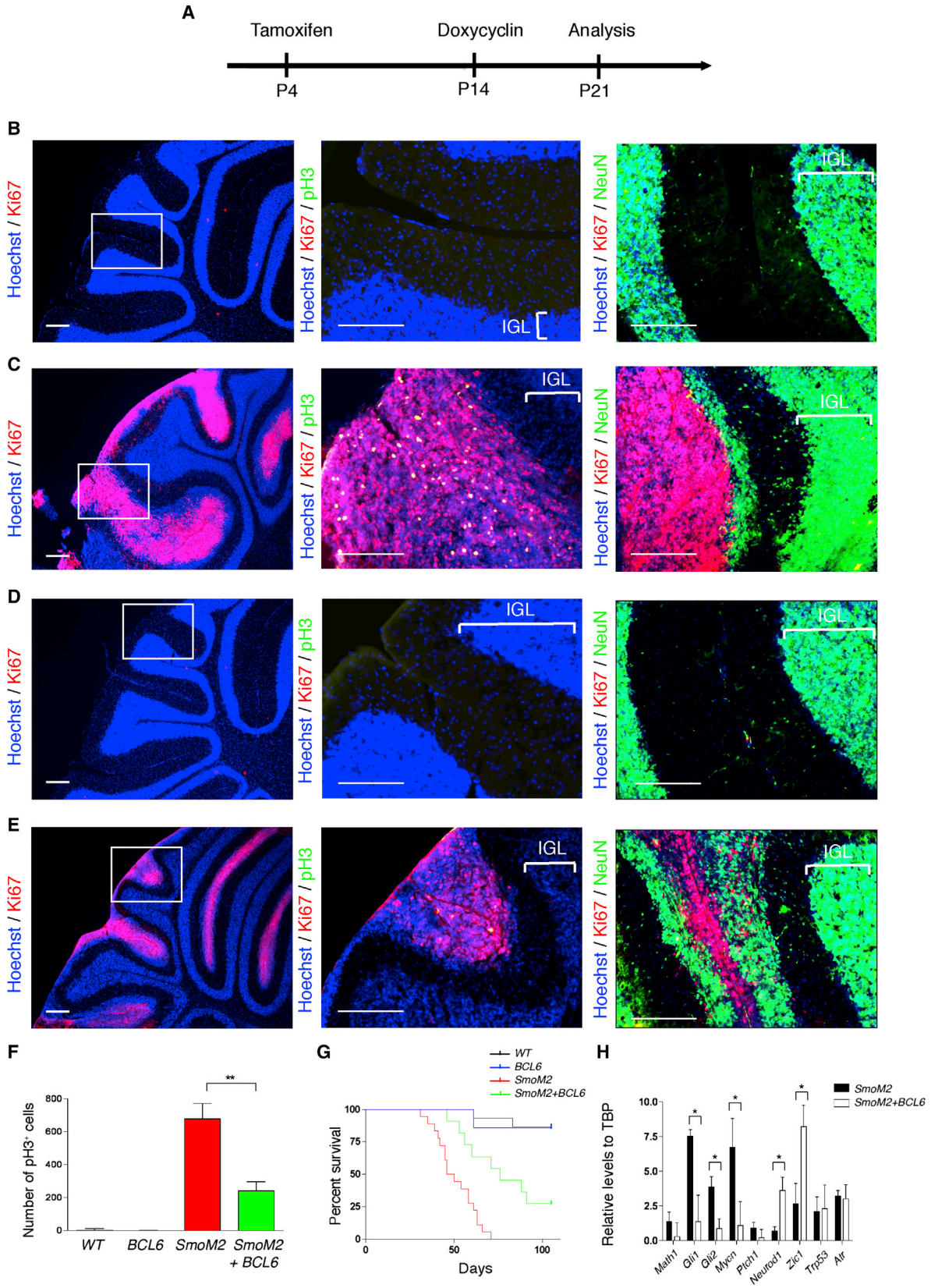

(legend on next page)

notably mirror those of MATH1/Atoh1, which is required for the specification and expansion of GNP as well as for MB tumorigenesis through the positive regulation of Gli factors (Flora et al., 2009).

In the context of normal brain development, our data point to BCL6 as an important component of proper neurogenesis, both in the cerebral and cerebellar cortex. Surprisingly, however, its molecular mechanism of action is completely distinct in the two brain regions: while in the cerebral cortex BCL6 acts mainly through inhibition of *Hes* genes downstream of the Notch pathway, in GNP it targets SHH effectors Gli1 and Gli2. This is consistent with the fact that the Notch pathway appears to have little impact on GNP neurogenesis, despite expression of *Hes* genes in these cells (Julian et al., 2010). Interestingly, the effect of BCL6 is conceptually the same in each case, i.e., it appears to act by decreasing the competence of neural progenitors to respond to proliferative/self-renewal signals (NOTCH or SHH), thereby promoting their neurogenic conversion.

In the context of oncogenic development, BCL6 stands out as it is both necessary for and capable of preventing MB development in vivo. Our finding that BCL6 requires BCOR for SHH signaling suppression in GNP is particularly relevant in the light of recent findings that *BCOR* is mutated in up to 7% of SHH MB cases (Kool et al., 2014; Northcott et al., 2012a; Olson, 2014; Pugh et al., 2012). Our data strongly suggest that *BCOR* mutations facilitate MB development through decreased repression of Gli1 and Gli2. Intriguingly, additional mutations were found in genes encoding other components of the N-COR complex, such as SMRT and LDB1 (Northcott et al., 2012a), suggesting that they could act in the same BCL6-dependent repressive complex. On the other hand, no mutations of *BCL6* were described in these studies centered on exonic regions, but *BCL6* expression previously was shown to be downregulated in SHH MB (Kho et al., 2004; Schüller et al., 2006). It will be interesting to explore which mechanisms, whether genetic or epigenetic, are responsible for BCL6 downregulation in MB, and to test whether the levels of expression and functionality of the BCL6/BCOR/SIRT1 complex may be relevant for the tailoring of treatments of SHH MB (Olson, 2014).

Our data and previous findings from others (Basso and Dalla-Favera, 2012) illustrate how the same factor can act as either an oncogene or a tumor suppressor, as previously shown for other proteins such as NOTCH1 (Radtke and Raj, 2003), MATH1 (Bossuyt et al., 2009; Flora et al., 2009), ZBTB7/Pokemon (Maeda et al., 2005; Wang et al., 2013), and HDAC1 (Santoro et al., 2013). Indeed *BCL6* is a well-established oncogene in some forms of B cell lymphoma (Phan and Dalla-Favera, 2004; Basso and Dalla-Favera, 2012). In this context, BCL6 is thought to act mainly through the transcriptional repression of genes involved in DNA damage sensing and apoptosis, in particular *TP53* and *ATR*, thus favoring persistent tolerance to DNA damage and, thereby, the accumulation of additional oncogenic mutations (Phan and Dalla-Favera, 2004; Basso and Dalla-Favera, 2012; Cerchietti et al., 2008; Hatzi and Melnick, 2014; Ranuncolo et al., 2007). Similarly BCL6 is involved in several forms of leukemia where BCL6-mediated repression of p53 was shown to promote leukemia stem cell survival (Duy et al., 2011; Hurtz et al., 2011). Interestingly, our data indicate that, in the case of cerebellar development and MB, p53 and ATR appeared to be unaffected by BCL6. The double-edged effects of BCL6 seem to be best explained by the fact that BCL6 represses a distinct set of transcriptional targets depending on the cellular context. It will be most interesting to dissect the underlying molecular mechanisms, which likely involve cell-specific chromatin modifiers or cofactors (Swaminathan et al., 2013), as these could be used in principle to suppress the ability of BCL6 to act in an oncogenic fashion in specific contexts.

The BCL6 dual effects could have additional clinical implications, since BCL6 inhibition using specific inhibitors was proposed as a therapeutic strategy for lymphoma (Robinson et al., 2012), but also some forms of leukemia (Duy et al., 2011). While it is unlikely that BCL6 inhibition would lead to MB in adult patients, since GNP are no longer present, future work should investigate whether BCL6 function is only required in GNP, and not postmitotic granule neurons, to prevent MB formation. Besides and notably, BCL6 inhibition also was proposed to be used against some forms of acute lymphoblastic leukemia (Duy et al., 2011), which include pediatric forms as well. On the other hand, while SHH MB could in principle be treated with SHH receptor antagonists (Ng and Curran, 2011; Rudin et al., 2009), they tend to acquire resistance to the treatment, mainly through mutations in SMO. The BCL6/BCOR/SIRT1 complex, by its capacity to block SHH signaling at the key level of *Gli1* and *Gli2* expression, may thus constitute an attractive target to activate in SHH-dependent tumors, which tend to acquire resistance to SHH receptor antagonists (Ng and Curran, 2011; Rudin et al., 2009).

EXPERIMENTAL PROCEDURES

Cell Culture

DAOY cell were purchased from ATCC (HTB-186) and were routinely propagated in Eagle's minimal essential medium (Invitrogen) supplemented with 10% (v/v) fetal bovine serum (Invitrogen) and 1% (v/v) penicillin/streptomycin (15070-063; Invitrogen). DAOY cells (1×10^6) were nucleofected with 10 μg of DNA using a Nucleofector 2b Device (Lonza) and Cell Line Nucleofector Kit VCA-1005 (Lonza), and plated onto coverslips in a 12-well plate (4×10^4

Figure 7. BCL6 Represses SHH MB Progression

(A) Schematic representation of the experimental protocol. Mice were injected with tamoxifen at P4, doxycyclin at P14, and analyzed at P21.

(B–E) Immunofluorescence staining for either Hoechst, Ki67, and pH3 or Hoechst, Ki67, and NeuN of sagittal sections of P21 WT (B), *SmoM2* (C), *tet-o-BCL6*$^+$ (D), or *SmoM2*;*tet-o-BCL6*$^+$ (E) mice after injection of tamoxifen at P4 and doxycyclin at P14.

(F) Quantification of pH 3$^+$ cells within the EGL at P21 in WT, *SmoM2*, *SmoM2*;*tet-o-BCL6*$^+$, and *tet-o-BCL6*$^+$ mice injected with tamoxifen at P4 and doxycyclin at P14; n = 4.

(G) Survival curve of WT (n = 15), *tet-o-BCL6*$^+$ (n = 7), *SmoM2* (n = 18), and *SmoM2*;*tet-o-BCL6*$^+$ (n = 13) mice injected with tamoxifen at P4 and doxycyclin at P14.

(H) Quantitative real-time PCR analysis for *Math1*, *Gli1*, *Gli2*, *Mycn*, *Ptch1*, *Neurod1*, *Zic1*, *Trp53*, and *Atr* from cerebellum of *SmoM2* and *SmoM2*;*tet-o-BCL6*$^+$ mice injected with tamoxifen at P4 and doxycyclin at P14; n = 3. All the mice are *Math1-creER*$^+$;*rtTA*$^+$.

Scale bars, 200 μm. Data are means ± SEM. *p < 0.05, **p < 0.01. See also Figure S7.

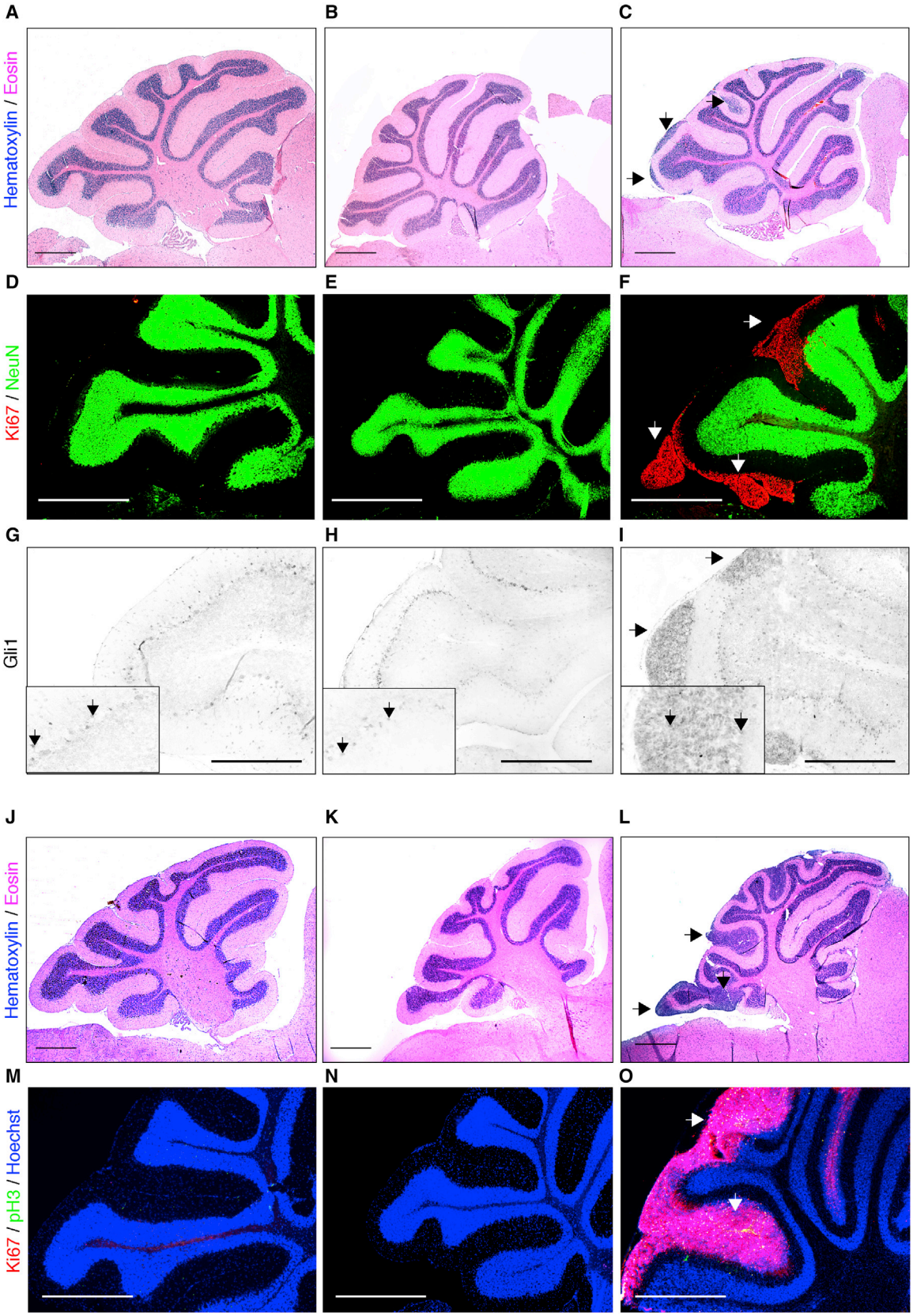

(legend on next page)

cells for each well). Cerebella from P7 mice were removed aseptically and incubated at 37°C with trypsin (Invitrogen) for 10 min. The trypsin was neutralized with PBS serum 10% and tissue was triturated using pipettes of decreasing bore size to obtain a single-cell suspension. The cells were centrifuged at room temperature and 1 × 10^6 cells were nucleofected with 10 μg of DNA using Nucleofector 2b Device (Lonza) and Mouse Neural Stem Cells Kit VPG-1004 (Lonza), and plated onto poly-L-lysine/laminin-coated coverslips in a 12-well plate (2 × 10^5 cells for each well). After nucleofection, the cells were maintained in neurobasal media (Invitrogen) supplemented with 1% (v/v) penicillin/streptomycin (Invitrogen), B27 (Invitrogen), and SHH-N (R&D Systems, 3 μg/ml). The cells were treated for 72 hr with 10 μM resveratrol (R5010, Sigma-Aldrich [Lagouge et al., 2006]). Additional details are available in the Supplemental Experimental Procedures.

Plasmids

The coding sequence of mouse BCL6 was amplified by PCR from cDNA, sequence verified, and cloned into pCAG-IRES-GFP (pCIG). The coding sequence of mouse Gli1 was amplified by PCR from cDNA and cloned into pCIG. The coding sequence of human BCOR was amplified by PCR from a plasmid of Dr. V.J. Bardwell (University of Minnesota) and cloned into pCIG. Truncated BCOR was amplified by PCR from WT BCOR. Double-stranded oligonucleotides coding for mouse *BCoR* 3′-UTR shRNA, human *BCOR* 3′-UTR shRNA, control shRNA, mouse *Gli1* shRNA, and mouse *Gli2* shRNA were cloned downstream of the *U6* promoter into the pSilencer2.1-CAG-Venus (pSCV2) plasmid according to the pSilencer instructions from Ambion. Additional details are available in the Supplemental Experimental Procedures.

Immunofluorescence Staining and Immunohistochemistry

Ex vivo cerebellar cells and DAOY cells were fixed in 4% paraformaldehyde in PBS (w/v) for 30 min and washed three times in PBS. P7, P14, P16, P21, P40, 12- and 20-week-old mice were anesthetized with an overdose of ketamine/xylazine and were fixed by perfusion with 4% paraformaldehyde in PBS; when appropriate, the cerebella were either cryoprotected in 30% (w/v) sucrose in water (Merck) or embedded in paraffin (brains were dehydrated with ethanol, then kept sequentially in ethanol/toluene, toluene/paraffin, and paraffin solutions). Immunofluorescence stainings were performed on slides with 20-μm-thick cryosections. Blocking solution consisted of PBS supplemented with 5% (v/v) horse serum (Invitrogen), 0.3% (v/v) Triton X-100 (Sigma), and 3% (w/v) BSA (Sigma). Antibody solution consisted of PBS supplemented with 1% horse serum, 0.1% (v/v) Triton X-100, and 3% BSA. Primary antibodies were incubated overnight at 4°C and secondary for 2 hr at 15°C–25°C. Nuclei were stained with bisbenzimide (Hoechst 33258; Sigma). Sections and coverslips were mounted with glycergel (Dako). Additional details are available in the Supplemental Experimental Procedures.

Western Blot, CoIP, ChIP, ChIP Quantitative PCR

Cerebella from P7 mice were removed aseptically and the cells were brought to a single cell suspension by pipetting in PBS. Western blot and coIP were performed on dissected P7 cerebellum. ChIP was performed as described previously (Tiberi et al., 2012) on dissected P7 cerebellum or DAOY cells. Additional details are available in the Supplemental Experimental Procedures.

RNA Isolation and Quantitative Real-Time PCR

For total RNA preparation, DAOY cells and cerebellum from mice were lysed in RNeasy lysis buffer + 1% (v/v) β-mercaptoethanol, and RNA was isolated using RNeasy RNA preparation minikit (QIAGEN) according to the manufacturer's instructions. Reverse transcription was done using Superscript II kit and protocol (Invitrogen). Quantitative PCR (qPCR) was performed in duplicate using Power SybrGreen Mix and a 7500 Real-Time PCR System (Applied Biosystems). Results are presented as linearized Ct values normalized to the housekeeping mouse *Tbp* and human *YWHAZ* and the indicated reference value ($2^{-\Delta\Delta Ct}$).

Flow Cytometry and Cell Sorting

Analytical FACS studies were carried out using an LSR Fortessa supported by the FACSDiva software (BD Biosciences). The PE-coupled cleaved caspase 3 staining was performed according to the manufacturer's recommendations (BD Pharmingen). Apoptosis positive control was obtained following cells treatment with either Okadaic acid 50 nM or Cisplatin 50 μM for 8 hr before analysis. Cell sorting was performed using a FACS Aria I cell sorter supported by the FACSDiva software (BD Biosciences). The cerebellum from *Math1-GFP*$^+$ mice was dissected out and manually dissociated in ice-cold dissociation buffer. Additional details are available in the Supplemental Experimental Procedures.

Mice

All mouse experiments were performed with the approval of the Université Libre de Bruxelles Committee for animal welfare. The *Bcl6*$^{+/-}$ mice, in which the null allele lacked exons 4–10, were a generous gift from R. Dalla-Favera (Columbia University) (Ye et al., 1997). The tet-o-BCL6 mice, in which human BCL6 expression was under the control of the tetracycline-responsive minimal promoter (20 copies), were a generous gift from B. Baron (University of Chicago) (Baron et al., 2004). The *Bcl6*$^{lox/lox}$ mice, in which the exons 7–9 of the *Bcl6* gene were flanked by *loxP* sites, were a generous gift from T. Takemori (RIKEN Research Center for Allergy and Immunology) (Kaji et al., 2012). *Math1-GFP* knockin mice (013593), *Math1-creERT2* (007684), *SmoM2* (005130), Rosa26-rtTA (006965), and *Trp53*$^{lox/lox}$ (008462) were purchased from The Jackson Laboratory. For EdU labeling, P7 mice were injected intraperitoneally (i.p.) with a single pulse (50 mg/kg of body weight) of EdU and killed after 24 hr. Tamoxifen (Sigma-Aldrich) was dissolved in warm corn oil (Sigma-Aldrich) and stored at −20°C. For conditional deletion of *Bcl6* and *Trp53*, pregnant females were i.p. injected with tamoxifen (0.5 mg) at E15.5. For induction of *SmoM2* expression, P4 pups were i.p. injected with tamoxifen (0.25 mg). Doxycyclin (Sigma-Aldrich) was dissolved in water and stored at −20°C. For *BCL6* transgene expression, P4 mice were i.p. injected with doxycyclin (0.5 mg).

SUPPLEMENTAL INFORMATION

Supplemental Information includes Supplemental Experimental Procedures, eight figures, and one table and can be found with this article online at http://dx.doi.org/10.1016/j.ccell.2014.10.021.

AUTHORS CONTRIBUTIONS

L.T., J.B., J.v.d.A., S. L., A.H., and A.B. performed all experiments. B.W.B. provided tet-o-BCL6 mice. L.T. and P.V. designed and analyzed all experiments and wrote the manuscript.

Figure 8. BCL6 Is Required to Suppress MB Development

(A–C) Hematoxylin and eosin staining of sagittal sections of cerebellum from 12-week-old *Math1-creER*$^+$;*Bcl6* WT;*Trp53* WT (A), *Math1-creER*$^+$;*Bcl6*$^{lox/lox}$;*Trp53* WT (B), and *Math1-creER*$^+$;*Bcl6*$^{lox/lox}$;*Trp53*$^{lox/lox}$ (C) mice. Scale bars, 500 μm. Arrows point to abnormal tissue.

(D–F) Immunofluorescence staining for NeuN and Ki67 of sagittal sections of cerebellum from 12-week-old *Math1-creER*$^+$;*Bcl6* WT;*Trp53* WT (D), *Math1-creER*$^+$;*Bcl6*$^{lox/lox}$;*Trp53* WT (E), and *Math1-creER*$^+$;*Bcl6*$^{lox/lox}$;*Trp53*$^{lox/lox}$ (F) mice. Scale bars, 500 μm.

(G–I) Immunohistochemistry staining of sagittal sections of cerebellum from 12-week-old *Math1-creER*$^+$;*Bcl6* WT;*Trp53* WT (G), *Math1-creER*$^+$;*Bcl6*$^{lox/lox}$;*Trp53* WT (H), and *Math1-creER*$^+$;*Bcl6*$^{lox/lox}$;*Trp53*$^{lox/lox}$ (I) mice with Gli1 antibody. Scale bars, 250 μm. Arrows point to Gli1$^+$ cells in higher magnification panels.

(J–L) Hematoxylin and eosin staining of sagittal sections of cerebellum from 20-week-old *Math1-creER*$^+$;*Bcl6* WT;*Trp53* WT (J), *Math1-creER*$^+$;*Bcl6*$^{lox/lox}$;*Trp53* WT (K), and *Math1-creER*$^+$;*Bcl6*$^{lox/lox}$;*Trp53*$^{lox/lox}$ (L) mice. Scale bars, 500 μm. Arrows point to abnormal tissue.

(M–O) Immunofluorescence staining for Hoechst, pH 3, and Ki67 of sagittal sections of cerebellum from 20-week-old *Math1-creER*$^+$;*Bcl6* WT;*Trp53* WT (M), *Math1-creER*$^+$;*Bcl6*$^{lox/lox}$;*Trp53* WT (N), and *Math1-creER*$^+$;*Bcl6*$^{lox/lox}$;*Trp53*$^{lox/lox}$ (O) mice. For all conditions, the pregnant females were injected with tamoxifen when the embryos were at E15.5.

Scale bars, 500 μm. Arrows point to abnormal tissue. See also Figure S8 and Table S1.

ACKNOWLEDGMENTS

We thank Gilbert Vassart, Bassem Hassan, Gianni Del Sal, and Jean-Christophe Marine for critically reading the manuscript; members of the lab and IRIBHM for helpful discussions and advice; and Jean-Marie Vanderwinden of the Light Microscopy Facility (LiMiF) for support with imaging. We thank Drs. Dalla-Favera and Takemori for providing us with BCL6 KO mice and Dr. Bardwell for providing us with BCOR cDNA.

This work was funded by grants from the Belgian Fonds de la Recherche Scientifique (FNRS), the Belgian Queen Elizabeth Medical Foundation, the Interuniversity Attraction Poles Program (IUAP), the WELBIO Program of the Walloon Region, the Fondation de Spoelbergh, and Fondation ULB (to P.V.). L.T. was supported by a Long Term European Molecular Biology Organization Fellowship, FNRS, and Télévie; and J.V was an Aspirant of the FNRS.

Received: March 28, 2014
Revised: July 27, 2014
Accepted: October 30, 2014
Published: December 8, 2014

REFERENCES

Alvarez-Rodríguez, R., and Pons, S. (2009). Expression of the proneural gene encoding Mash1 suppresses MYCN mitotic activity. J. Cell Sci. *122*, 595–599.

Asselin-Labat, M.L., Sutherland, K.D., Barker, H., Thomas, R., Shackleton, M., Forrest, N.C., Hartley, L., Robb, L., Grosveld, F.G., van der Wees, J., et al. (2007). Gata-3 is an essential regulator of mammary-gland morphogenesis and luminal-cell differentiation. Nat. Cell Biol. *9*, 201–209.

Baron, B.W., Anastasi, J., Montag, A., Huo, D., Baron, R.M., Karrison, T., Thirman, M.J., Subudhi, S.K., Chin, R.K., Felsher, D.W., et al. (2004). The human BCL6 transgene promotes the development of lymphomas in the mouse. Proc. Natl. Acad. Sci. USA *101*, 14198–14203.

Basso, K., and Dalla-Favera, R. (2012). Roles of BCL6 in normal and transformed germinal center B cells. Immunol. Rev. *247*, 172–183.

Batlle, E., Bacani, J., Begthel, H., Jonkheer, S., Gregorieff, A., van de Born, M., Malats, N., Sancho, E., Boon, E., Pawson, T., et al. (2005). EphB receptor activity suppresses colorectal cancer progression. Nature *435*, 1126–1130.

Ben-Arie, N., Bellen, H.J., Armstrong, D.L., McCall, A.E., Gordadze, P.R., Guo, Q., Matzuk, M.M., and Zoghbi, H.Y. (1997). Math1 is essential for genesis of cerebellar granule neurons. Nature *390*, 169–172.

Bossuyt, W., Kazanjian, A., De Geest, N., Van Kelst, S., De Hertogh, G., Geboes, K., Boivin, G.P., Luciani, J., Fuks, F., Chuah, M., et al. (2009). Atonal homolog 1 is a tumor suppressor gene. PLoS Biol. *7*, e39.

Cerchietti, L.C., Polo, J.M., Da Silva, G.F., Farinha, P., Shaknovich, R., Gascoyne, R.D., Dowdy, S.F., and Melnick, A. (2008). Sequential transcription factor targeting for diffuse large B-cell lymphomas. Cancer Res. *68*, 3361–3369.

Chang, C.C., Ye, B.H., Chaganti, R.S., and Dalla-Favera, R. (1996). BCL-6, a POZ/zinc-finger protein, is a sequence-specific transcriptional repressor. Proc. Natl. Acad. Sci. USA *93*, 6947–6952.

Cho, J.H., and Tsai, M.J. (2006). Preferential posterior cerebellum defect in BETA2/NeuroD1 knockout mice is the result of differential expression of BETA2/NeuroD1 along anterior-posterior axis. Dev. Biol. *290*, 125–138.

Corrales, J.D., Blaess, S., Mahoney, E.M., and Joyner, A.L. (2006). The level of sonic hedgehog signaling regulates the complexity of cerebellar foliation. Development *133*, 1811–1821.

Dahmane, N., and Ruiz i Altaba, A. (1999). Sonic hedgehog regulates the growth and patterning of the cerebellum. Development *126*, 3089–3100.

Duy, C., Hurtz, C., Shojaee, S., Cerchietti, L., Geng, H., Swaminathan, S., Klemm, L., Kweon, S.M., Nahar, R., Braig, M., et al. (2011). BCL6 enables Ph+ acute lymphoblastic leukaemia cells to survive BCR-ABL1 kinase inhibition. Nature *473*, 384–388.

Emmenegger, B.A., Hwang, E.I., Moore, C., Markant, S.L., Brun, S.N., Dutton, J.W., Read, T.A., Fogarty, M.P., Singh, A.R., Durden, D.L., et al. (2013). Distinct roles for fibroblast growth factor signaling in cerebellar development and medulloblastoma. Oncogene *32*, 4181–4188.

Flora, A., Klisch, T.J., Schuster, G., and Zoghbi, H.Y. (2009). Deletion of Atoh1 disrupts Sonic Hedgehog signaling in the developing cerebellum and prevents medulloblastoma. Science *326*, 1424–1427.

Fuccillo, M., Joyner, A.L., and Fishell, G. (2006). Morphogen to mitogen: the multiple roles of hedgehog signalling in vertebrate neural development. Nat. Rev. Neurosci. *7*, 772–783.

Gilbertson, R.J., and Ellison, D.W. (2008). The origins of medulloblastoma subtypes. Annu. Rev. Pathol. *3*, 341–365.

Grimmer, M.R., and Weiss, W.A. (2008). BMPs oppose Math1 in cerebellar development and in medulloblastoma. Genes Dev. *22*, 693–699.

Hatzi, K., and Melnick, A. (2014). Breaking bad in the germinal center: how deregulation of BCL6 contributes to lymphomagenesis. Trends Mol. Med. *20*, 343–352.

Hochedlinger, K., Yamada, Y., Beard, C., and Jaenisch, R. (2005). Ectopic expression of Oct-4 blocks progenitor-cell differentiation and causes dysplasia in epithelial tissues. Cell *121*, 465–477.

Hurtz, C., Hatzi, K., Cerchietti, L., Braig, M., Park, E., Kim, Y.M., Herzog, S., Ramezani-Rad, P., Jumaa, H., Müller, M.C., et al. (2011). BCL6-mediated repression of p53 is critical for leukemia stem cell survival in chronic myeloid leukemia. J. Exp. Med. *208*, 2163–2174.

Huynh, K.D., and Bardwell, V.J. (1998). The BCL-6 POZ domain and other POZ domains interact with the co-repressors N-CoR and SMRT. Oncogene *17*, 2473–2484.

Huynh, K.D., Fischle, W., Verdin, E., and Bardwell, V.J. (2000). BCoR, a novel corepressor involved in BCL-6 repression. Genes Dev. *14*, 1810–1823.

Jeong, J., Mao, J., Tenzen, T., Kottmann, A.H., and McMahon, A.P. (2004). Hedgehog signaling in the neural crest cells regulates the patterning and growth of facial primordia. Genes Dev. *18*, 937–951.

Jones, D.T., Jäger, N., Kool, M., Zichner, T., Hutter, B., Sultan, M., Cho, Y.J., Pugh, T.J., Hovestadt, V., Stütz, A.M., et al. (2012). Dissecting the genomic complexity underlying medulloblastoma. Nature *488*, 100–105.

Julian, E., Dave, R.K., Robson, J.P., Hallahan, A.R., and Wainwright, B.J. (2010). Canonical Notch signaling is not required for the growth of Hedgehog pathway-induced medulloblastoma. Oncogene *29*, 3465–3476.

Kaji, T., Ishige, A., Hikida, M., Taka, J., Hijikata, A., Kubo, M., Nagashima, T., Takahashi, Y., Kurosaki, T., Okada, M., et al. (2012). Distinct cellular pathways select germline-encoded and somatically mutated antibodies into immunological memory. J. Exp. Med. *209*, 2079–2097.

Kho, A.T., Zhao, Q., Cai, Z., Butte, A.J., Kim, J.Y., Pomeroy, S.L., Rowitch, D.H., and Kohane, I.S. (2004). Conserved mechanisms across development and tumorigenesis revealed by a mouse development perspective of human cancers. Genes Dev. *18*, 629–640.

Kool, M., Jones, D.T., Jäger, N., Northcott, P.A., Pugh, T.J., Hovestadt, V., Piro, R.M., Esparza, L.A., Markant, S.L., Remke, M., et al.; ICGC PedBrain Tumor Project (2014). Genome sequencing of SHH medulloblastoma predicts genotype-related response to smoothened inhibition. Cancer Cell *25*, 393–405.

Kouros-Mehr, H., Bechis, S.K., Slorach, E.M., Littlepage, L.E., Egeblad, M., Ewald, A.J., Pai, S.Y., Ho, I.C., and Werb, Z. (2008). GATA-3 links tumor differentiation and dissemination in a luminal breast cancer model. Cancer Cell *13*, 141–152.

Lagouge, M., Argmann, C., Gerhart-Hines, Z., Meziane, H., Lerin, C., Daussin, F., Messadeq, N., Milne, J., Lambert, P., Elliott, P., et al. (2006). Resveratrol improves mitochondrial function and protects against metabolic disease by activating SIRT1 and PGC-1alpha. Cell *127*, 1109–1122.

Machold, R., and Fishell, G. (2005). Math1 is expressed in temporally discrete pools of cerebellar rhombic-lip neural progenitors. Neuron *48*, 17–24.

Maeda, T., Hobbs, R.M., Merghoub, T., Guernah, I., Zelent, A., Cordon-Cardo, C., Teruya-Feldstein, J., and Pandolfi, P.P. (2005). Role of the proto-oncogene Pokemon in cellular transformation and ARF repression. Nature *433*, 278–285.

Marino, S., Vooijs, M., van Der Gulden, H., Jonkers, J., and Berns, A. (2000). Induction of medulloblastomas in p53-null mutant mice by somatic inactivation

of Rb in the external granular layer cells of the cerebellum. Genes Dev. *14*, 994–1004.

Min, S.W., Cho, S.H., Zhou, Y., Schroeder, S., Haroutunian, V., Seeley, W.W., Huang, E.J., Shen, Y., Masliah, E., Mukherjee, C., et al. (2010). Acetylation of tau inhibits its degradation and contributes to tauopathy. Neuron *67*, 953–966.

Nahar, R., Ramezani-Rad, P., Mossner, M., Duy, C., Cerchietti, L., Geng, H., Dovat, S., Jumaa, H., Ye, B.H., Melnick, A., and Müschen, M. (2011). Pre-B cell receptor-mediated activation of BCL6 induces pre-B cell quiescence through transcriptional repression of MYC. Blood *118*, 4174–4178.

Ng, J.M., and Curran, T. (2011). The Hedgehog's tale: developing strategies for targeting cancer. Nat. Rev. Cancer *11*, 493–501.

Northcott, P.A., Jones, D.T., Kool, M., Robinson, G.W., Gilbertson, R.J., Cho, Y.J., Pomeroy, S.L., Korshunov, A., Lichter, P., Taylor, M.D., and Pfister, S.M. (2012a). Medulloblastomics: the end of the beginning. Nat. Rev. Cancer *12*, 818–834.

Northcott, P.A., Korshunov, A., Pfister, S.M., and Taylor, M.D. (2012b). The clinical implications of medulloblastoma subgroups. Nat Rev Neurol *8*, 340–351.

Olson, J.M. (2014). Therapeutic opportunities for medulloblastoma come of age. Cancer Cell *25*, 267–269.

Parsons, D.W., Li, M., Zhang, X., Jones, S., Leary, R.J., Lin, J.C., Boca, S.M., Carter, H., Samayoa, J., Bettegowda, C., et al. (2011). The genetic landscape of the childhood cancer medulloblastoma. Science *331*, 435–439.

Phan, R.T., and Dalla-Favera, R. (2004). The BCL6 proto-oncogene suppresses p53 expression in germinal-centre B cells. Nature *432*, 635–639.

Pugh, T.J., Weeraratne, S.D., Archer, T.C., Pomeranz Krummel, D.A., Auclair, D., Bochicchio, J., Carneiro, M.O., Carter, S.L., Cibulskis, K., Erlich, R.L., et al. (2012). Medulloblastoma exome sequencing uncovers subtype-specific somatic mutations. Nature *488*, 106–110.

Radtke, F., and Raj, K. (2003). The role of Notch in tumorigenesis: oncogene or tumour suppressor? Nat. Rev. Cancer *3*, 756–767.

Ranuncolo, S.M., Polo, J.M., Dierov, J., Singer, M., Kuo, T., Greally, J., Green, R., Carroll, M., and Melnick, A. (2007). Bcl-6 mediates the germinal center B cell phenotype and lymphomagenesis through transcriptional repression of the DNA-damage sensor ATR. Nat. Immunol. *8*, 705–714.

Robinson, G., Parker, M., Kranenburg, T.A., Lu, C., Chen, X., Ding, L., Phoenix, T.N., Hedlund, E., Wei, L., Zhu, X., et al. (2012). Novel mutations target distinct subgroups of medulloblastoma. Nature *488*, 43–48.

Romer, J.T., Kimura, H., Magdaleno, S., Sasai, K., Fuller, C., Baines, H., Connelly, M., Stewart, C.F., Gould, S., Rubin, L.L., and Curran, T. (2004). Suppression of the Shh pathway using a small molecule inhibitor eliminates medulloblastoma in Ptc1(+/-)p53(-/-) mice. Cancer Cell *6*, 229–240.

Rose, M.F., Ren, J., Ahmad, K.A., Chao, H.T., Klisch, T.J., Flora, A., Greer, J.J., and Zoghbi, H.Y. (2009). Math1 is essential for the development of hindbrain neurons critical for perinatal breathing. Neuron *64*, 341–354.

Roussel, M.F., and Hatten, M.E. (2011). Cerebellum development and medulloblastoma. Curr. Top. Dev. Biol. *94*, 235–282.

Rudin, C.M., Hann, C.L., Laterra, J., Yauch, R.L., Callahan, C.A., Fu, L., Holcomb, T., Stinson, J., Gould, S.E., Coleman, B., et al. (2009). Treatment of medulloblastoma with hedgehog pathway inhibitor GDC-0449. N. Engl. J. Med. *361*, 1173–1178.

Sakano, D., Kato, A., Parikh, N., McKnight, K., Terry, D., Stefanovic, B., and Kato, Y. (2010). BCL6 canalizes Notch-dependent transcription, excluding Mastermind-like1 from selected target genes during left-right patterning. Dev. Cell *18*, 450–462.

Santoro, F., Botrugno, O.A., Dal Zuffo, R., Pallavicini, I., Matthews, G.M., Cluse, L., Barozzi, I., Senese, S., Fornasari, L., Moretti, S., et al. (2013). A dual role for Hdac1: oncosuppressor in tumorigenesis, oncogene in tumor maintenance. Blood *121*, 3459–3468.

Schüller, U., Kho, A.T., Zhao, Q., Ma, Q., and Rowitch, D.H. (2006). Cerebellar 'transcriptome' reveals cell-type and stage-specific expression during postnatal development and tumorigenesis. Mol. Cell. Neurosci. *33*, 247–259.

Schüller, U., Heine, V.M., Mao, J., Kho, A.T., Dillon, A.K., Han, Y.G., Huillard, E., Sun, T., Ligon, A.H., Qian, Y., et al. (2008). Acquisition of granule neuron precursor identity is a critical determinant of progenitor cell competence to form Shh-induced medulloblastoma. Cancer Cell *14*, 123–134.

Snuderl, M., Batista, A., Kirkpatrick, N.D., Ruiz de Almodovar, C., Riedemann, L., Walsh, E.C., Anolik, R., Huang, Y., Martin, J.D., Kamoun, W., et al. (2013). Targeting placental growth factor/neuropilin 1 pathway inhibits growth and spread of medulloblastoma. Cell *152*, 1065–1076.

Swaminathan, S., Huang, C., Geng, H., Chen, Z., Harvey, R., Kang, H., Ng, C., Titz, B., Hurtz, C., Sadiyah, M.F., et al. (2013). BACH2 mediates negative selection and p53-dependent tumor suppression at the pre-B cell receptor checkpoint. Nat. Med. *19*, 1014–1022.

Taipale, J., and Beachy, P.A. (2001). The Hedgehog and Wnt signalling pathways in cancer. Nature *411*, 349–354.

Thompson, M.C., Fuller, C., Hogg, T.L., Dalton, J., Finkelstein, D., Lau, C.C., Chintagumpala, M., Adesina, A., Ashley, D.M., Kellie, S.J., et al. (2006). Genomics identifies medulloblastoma subgroups that are enriched for specific genetic alterations. J. Clin. Oncol. *24*, 1924–1931.

Tiberi, L., van den Ameele, J., Dimidschstein, J., Piccirilli, J., Gall, D., Herpoel, A., Bilheu, A., Bonnefont, J., Iacovino, M., Kyba, M., et al. (2012). BCL6 controls neurogenesis through Sirt1-dependent epigenetic repression of selective Notch targets. Nat. Neurosci. *15*, 1627–1635.

Wang, X., Venugopal, C., Manoranjan, B., McFarlane, N., O'Farrell, E., Nolte, S., Gunnarsson, T., Hollenberg, R., Kwiecien, J., Northcott, P., et al. (2012). Sonic hedgehog regulates Bmi1 in human medulloblastoma brain tumor-initiating cells. Oncogene *31*, 187–199.

Wang, G., Lunardi, A., Zhang, J., Chen, Z., Ala, U., Webster, K.A., Tay, Y., Gonzalez-Billalabeitia, E., Egia, A., Shaffer, D.R., et al. (2013). Zbtb7a suppresses prostate cancer through repression of a Sox9-dependent pathway for cellular senescence bypass and tumor invasion. Nat. Genet. *45*, 739–746.

Wetmore, C., Eberhart, D.E., and Curran, T. (2001). Loss of p53 but not ARF accelerates medulloblastoma in mice heterozygous for patched. Cancer Res. *61*, 513–516.

Yang, Z.J., Ellis, T., Markant, S.L., Read, T.A., Kessler, J.D., Bourboulas, M., Schüller, U., Machold, R., Fishell, G., Rowitch, D.H., et al. (2008). Medulloblastoma can be initiated by deletion of Patched in lineage-restricted progenitors or stem cells. Cancer Cell *14*, 135–145.

Ye, B.H., Lista, F., Lo Coco, F., Knowles, D.M., Offit, K., Chaganti, R.S., and Dalla-Favera, R. (1993). Alterations of a zinc finger-encoding gene, BCL-6, in diffuse large-cell lymphoma. Science *262*, 747–750.

Ye, B.H., Cattoretti, G., Shen, Q., Zhang, J., Hawe, N., de Waard, R., Leung, C., Nouri-Shirazi, M., Orazi, A., Chaganti, R.S., et al. (1997). The BCL-6 proto-oncogene controls germinal-centre formation and Th2-type inflammation. Nat. Genet. *16*, 161–170.

Zhao, H., Ayrault, O., Zindy, F., Kim, J.H., and Roussel, M.F. (2008). Post-transcriptional down-regulation of Atoh1/Math1 by bone morphogenic proteins suppresses medulloblastoma development. Genes Dev. *22*, 722–727.